Sorafenib encapsulation in nanostructured polymeric matrixes and their evaluation in hepatocellular carcinoma

MSc in Molecular and Cell Biology

Final Master'sThesis

Author: Cristina Novillo Ibáñez

Director: Dr. Miguel Ángel de Gregorio Ariza

Ponente: María Fillat Castejón

December 2016

[Escr
corto
desc

Universidad Zaragoza

Instituto Universitario de Investigación en Nanociencia de Aragón
Universidad Zaragoza

IIS Aragón
Instituto de Investigación Sanitaria Aragón

a

“As a scientist I had a unique opportunity to change things.”

Bertolt Brecht, The Life of Galilei

THANKS

I would dearly like to thank my tutor Manuel Arruebo and my supervisor Vanesa Andreu for their truly invaluable guidance and scientific advice, and also all my colleagues in the NPF and PMD groups for their daily support. I would also like to thank Loreto Escorihuela for her emotional counseling and my family, specially my mother and my aunt, for their continuous surveillance upon my health. Lastly, my thanks go to my best friends, in whatever part of the world they happen to be, who have aided me both emotional- and academically.

ABBREVIATIONS

AASLD = American Association for the Study of Liver Diseases

ATP = Adenosin Tri-Phosphate

BCLC = Barcelona Clinic Liver Cancer

CPP = Cell Penetrating Peptides

CT = Computer Tomography

DGA = Diputación General de Aragón

DLS = Dynamic Light Scattering

DMSO = dymethil sulfoxide

DPBS = Dulbecco's Phosphate Buffered Saline

DSC =Differential Scanning Calorimetry

EASL = European Association for the Study of the Liver

EDC = *N*-(3-Dimethylaminopropyl)-*N*'-ethylcarbodiimide

EGF(R) = Epidermal Growth Factor (Receptor)

EMA = European Medicament Agency

EMEM = Eagle's Minimum Essential Medium

EPR effect = Enhanced Permeability and Retention Effect

FDA = Food and Drug Administration

FGF(R) = Fibroblas Growth Factor (Receptor)

FR = Folic Acid Receptor

FTIR = Fourier Transform Infrared Spectroscopy

GFP = Green Fluorescent Protein

HBV = Hepatitis B Virus

HCC = Hepatocellular Carcinoma

HCV =Hepatitis C Virus

IGFR =

IL8 = Interleukin 8

Kcps = Kilo Counts per Second

MDR = Multi-drug resistance

MES = 4-Morpholineethanesulfonic

MRI = Magnetic Resonance Imaging

MW96 =-Multiwell Plate with 96 Wells

NEAA = non-essential aminoacids

NHS = *N*-Hydroxysuccinimide

O/W = Oil-in-water

OS = Overall Survival

PDGF(R) = Platelet-Derived Growth Factor (Receptor)

pDNA = plasmidic Deoxyribonucleic Acids

PEG = Poly-ethilene Glycol

PEI = Polyethileinimine

PLGA = Poly-Lactic-Glycolic Acid

PCR = Polymerase Chain Reaction

Poly-HIS = Polyhistidine

RFA = Radiofrequency Ablation

shRNA = small hairpin Ribonucleic Acid

siRNA = small interfering Ribonucleic Acids

Srf = Sorafenib

TACE = Trans-arterial chemoembolization

TEM = Transmission Electron Microscopy

TfR = Transferrin Receptor

TNF = Tumor Necrosis Factor

TTP = Time to Tumor Progression

US = Ultrasonography

VEGF(R) = Vascular-Endothelial Growth Factor (Receptor)

XPS = X-Ray Photoelectron spectroscopy

INDEX

ABSTRACT

Hepatocellular carcinoma (HCC) is the fifth most common cancer worldwide, and it is usually diagnosed at advanced stages when only systemic therapy is feasible. Current systemic therapy relies on the chemotherapeutical agent Sorafenib, a highly hydrophobic compound that hinders angiogenesis and proliferation in the tumor vasculature and the tumoral cells, respectively. However, Sorafenib achieves a limited survival rate increase and normally produces severe side effects. In this sense, we have developed biodegradable PLGA-based Sorafenib bearing nanoparticles further enhanced by the attachment of the polymer PEI, which provides it with a mechanism for endosomal escape and serves as a platform for gene therapy. As adaptation to hypoxia is a critical step in tumor progression, we want to direct gene therapy against HIF-1α, a factor promoting cell survival in hypoxic conditions. Moreover, we have proved the low cytotoxicity that our nanoparticles exert in HCC cells.

INTRODUCTION

Cancer is one of the leading causes of death worldwide. Among the wide range of pathologies the term "cancer" includes, hepatocellular carcinoma (HCC), commonly named as "liver cancer", which is one of the most prevalent (the fifth most common type of cancer in the world), most aggressive and with worst prognosis. 3-year survival ratio in untreated patients with early HCC is 50%, while most patients diagnosed with advanced HCC left untreated survive less than six months. In addition, its prevalence is higher in subsaharian Africa and the east of Asia, due to a higher hepatitits B virus (HBV) infection rate [1].

Early diagnose is the best way to achieve a successful treatment. Ultrasonography (US) is the diagnostic technique recommended by the European Association for the Study of the Liver (EASL) and the American Association for the Study of Liver disease for the diagnose of HCC, although computer tomography (CT) scanning and magnetic resonance imaging (MRI) are also available [2].

Prevalence in the south of Europe, including Spain, is 9,8 cases for 100.000 inhabitants, which is higher than in other zones of the European continent, with 2,6 cases in North Europe and 5,8 in East and Central Europe. Despite the availability of diagnose alternatives, it is usually a fatal disease, given that up to 70% cases are diagnosed in an advanced phase, when no curative treatment (such as surgical resection) may be applied. A multricentric study carried out in Spain revealed that only 49,5% of the patients were diagnosed in the initial phases BCLC (Barcelona Clinic Liver Cancer) 0 or A, and those who had already lost liver functionality (Child-Pugh B)[3] had a worse prognosis and suffered graver side-effects than those who still preserved it, leading in 49% patients to treatment withdrawal [4].

Hepatocarcinogenesis is a multistep process in which genetic changes occurring in either hepatocytes or their stem cells lead to a higher proliferation rate and neoplasia. Here we will briefly describe the main pathways involved in HCC genesis [5].

- MAPK pathway: The Raf/MAPK/extracellular-signal-regulated kinase (ERK) pathway transduces extracellular signals from tyrosine kinase receptors bound to the cell membrane to transcription factors entering the nucleus and exerting their transcriptional activity. These receptors include IGFR, VEGFR and PDGFR. Ligand biding results in kinase activation and receptor phosphorylation. Activation of the GRB2/SHC/SOS adapter molecule follows, which in turn activates the MEK protein, triggering a cascade of phosphorylation events, being the small GTPase Ras and the serin/threonin kinase Raf the key regulators, and ultimately leading to the activation of several molecules related to cell proliferation and cell survival.
- PI3K/AKT/mTOR pathway: the binding of growth factors (IGF, EGF) to their receptors activates PI3K, which in turn produces PIP3b, a lipidic-nature secondary messenger. PIP3b triggers activity of the serine/threonine kinase AKT, leading to phosphorylation of mTOR and BCL-2. mTOR increases proliferation, and BLC-2 acts as an antiapoptotic

signal. In healthy tissue, the suppressor PTEN targets PIP3b for dephosphorylation, but abnormalities lead to a PTEN loss of function, causing a constitutive activation of this pathway. In addition, IGF and its receptor are both commonly upregulated in HCC. Decreased PTEN levels have been correlated to a worse prognosis and to a reduced overall survival (OS).

- VEGF/VEGFR, PDGFR and FGFR: in healthy tissues a balance in maintained between pro- and anti-angiogenic factors to promote angiogenesis only when necessary. However, HCC is known to be a high angiogenic tumor, what occurs through the upregulation of pro-angiogenic factors such as VEGF, angiopoietin, PDGF, TGF, FGF and EGF. In addition, some of these molecules activate both RAF/MEK/ERK and PI3k/AKT/mTOR pathways, bridging angiogenesis with reduced apoptosis and cell proliferation. High levels of VEGF have been linked with HCC progression, poor outcome after resection, disease recurrence, reduced OS and vascular invasion. FGF-2 levels are also higher in patients suffering from HCC, and it has been correlated with a higher tumor microvessel density (TMD) and disease recurrence.
- WNT/β.catenin pathway: abnormal transcription pattern of the transcription factor β.catenin leads to its translocation into the nucleus: Hepatocytes exhibiting high levels of β.catenin into the nucleus have a higher proliferation rate and a differential HCC-like membrane protein profile, along with metastatic behavior. A high incidence of β.catenin mutations (around 40%) has been observed in hepatitis-C virus (HCV)- driven HCC. During normal homeostasis, Wnt proteins are absent, but upon Wnt signaling β.catenin is dephosphorylated and thus its degradation is impaired.

The risk factors for the development of HCC are multiple, including medical, genetic and environmental factors. Cirrhosis of any etiology is considered to be the main risk factor for HCC; cirrhosis is present in more than 70% of the patients with primary liver cancer. Following this, HBV infection heavily promotes HCC. 50% of HCC patients do host HBV. The degree of viremia and the length of its duration negatively affect the rate of occurrence and predispose to a worse prognosis. The virus genotype also affects prevalence: HBV genotype A, most prevalent in African populations, and genotype B, which can be found especially among Asian patients, are associated with an increased rate of HCC. HBV integrates into the host genome causing chromosome instability and insertional mutations, a process that can lead to the activation of various oncogenes, such as cyclin A. Additionally, the HBx viral protein (among others) acts as a transactivator to upregulate some oncogenes, for example the transcription factor NF-κβ, and other molecules promoting tumor progression, such as IL-8, TNF, or EFGR. HBx can also stimulate several molecular pathways affected upon tumor development. The risk is even higher for those who simultaneously have HBV and cirrhosis. Hepatitis C virus (HCV) also promotes HCC development through the action of several viral proteins, including core, NS3 and NS5A proteins. The core-forming protein interacts with p53 and upregulates Wnt-1 pathway at the transcriptional level. Hepatitis C virus (HCV)-associated cirrhosis is the major cause of HCC in Japan, North and Latin America and Europe. Patients suffering from Diabetes mellitus display a higher HCC incidence too. Environmental factors do also play a role in development of HCC: it has been stated that both alcohol and cigarette consumption lead to a higher relative risk. A family history of liver cancer, particularly among first-degree relatives, also promotes HCC development in HBV-infected individuals [5,6].

Nowadays there are multiple available treatments for HCC, including surgical resection, TACE, radiotherapy, chemotherapy, etc… which application depends primarily on the cancer developmental stage. When tumor size is still small and no metastasis has yet occurred, the most common therapeutic choice is hepatic surgical resection. It is also required that the patient has not developed cirrhosis and that the liver is functional (Child-Pugh A). As HCC in early stages is mainly supplied by the portal vein, its embolization successfully leads to tumor reduction. Laparoscopic liver resection is also increasing in popularity, given that both costs and chirurgical risks are lower than in open resection and results are comparable [1]. Liver transplant is also an option, especially for those who experience HCC recurrence or liver failure[1].

However, as already stated, due to the low symptomatology this pathology produces, most cases are detected in an advanced stage, what leaves solely non-curative treatments as open options. Within this category, ablation through ethanol injection or radiofrequency/microwave application are quite limited, mainly because of potential ethanol leaks and excessive tumor size, respectively. TACE (Trans-arterial chemoembolization) is one of the most preferred techniques within the non-curative range. TACE consists in embolizing tumor-supplying blood vessels directly with drugs (cTACE) or via drug-eluting beads (DEB TACE), in which tumor is depleted of blood flow and simultaneously attacked by a chemotherapeutic agent. Doxorubicin and cisplatin are the drugs most frequently used [1]. These are all locoregional therapies, but systemic therapies such as chemotherapy are still widely prescribed. The only FDA- and EMA-approved systemic treatment for advanced HCC is Sorafenib (Srf), a chemotherapeutic agent commercialized under the name of Nexavar® by Bayer Healthcare [1].

Srf was discovered between 1989 and 1999 through screening and later improvement of neosynthesized drugs. Throughout the 20th century efforts to find drugs against cancer focused on untargeted drug synthesis. However, the discovery of many cancer-driven deregulations in molecular pathways, such as MAPKinases, Raf, Ras, mTOR, ERK or β-catenin, shifted research towards molecular targeting. Srf was aimed to target Raf serin/threonin kinase. Deregulated signaling through Raf kinase isoforms is detected in around 30% of human cancers (RAF/MEK/ERK pathway, see above). Constitutively active Raf kinase through ras mutation is found in up to 30% of HCC. Raf1 hyperactivation without a causing oncogenic mutation is also common in HCC. Thus, Raf was selected as a drug target for a HTS screening, which rendered 3-thienyl urea 1 as a promising compound, whose effect was later improved tenfold by addition of a methyl substitution in the phenyl ring. A wide library comprising around 1000 variants of this compound was then constructed and screened against Raf1. Replacing its distal ring with a 4 pyridyl moiety increased its potency by fivefold. Finally, modification of this pyridyl moiety led to the identification of Sorafenib, which 4-pyridil ring occupies the ATP adenine binding pocket of the kinase domain. Further *in vitro* tests proved that Srf not only inhibited Raf isoforms, but also several other kinases involved in tumor genesis, such as PDGFR, VEGFR, FGFR, c-kit and Flt-3 [7].

Srf was *in vitro* and *in vivo* tested in a wide variety of tumors: colon carcinoma, breast carcinoma, leukemia cells… However it was in RCC and HCC that the best results were obtained, and therefore the ones that accessed clinical trials. For a review on RCC first clinical

trials, please consult Wilhelm *et al*, 2006 [7]. Regarding HCC, two large-scale, placebo controlled, randomized comparative studies were performed in patients with advanced HCC, namely the SHARP and the Asia-Pacific (2008 and 2009, respectively) studies. Both showed an increased disease control rate, longer survival period and a 30% decrease in the risk of death. The SHARP study reported an increase of approximately of 3 months in the OS (Placebo OS was 7,9 months while Srf OS was 10,7 months). Time to tumor progression (TTP) was also improved in both trials. Even though some clinical trials combining Srf with other antiangiogenic agents, such as Brivanib, Linifanib, or Ramucirumab, have been carried out, Srf remains up to date the only FDA-approved treatment for HCC stage C patients according to the BCLC[3] , and both the guidelines of the European Association for the Study of Liver (EASL) and that of the American Association for the Study of Liver Diseases (AASLD) recommend Srf as a first-line treatment for advanced HCC .

Srf is a tyrosine- and serin/threonin-kinase inhibitor that acts primarily against angiogenic factor receptors, such as VEGFR and PDGFR, and against cell signaling proteins like Raf and c-Kit. VEGFR and PDGFR are involved in the solid tumor-associated angiogenesis, which requires the expansion of the patient's liver capillary vessels to develop further growth, and which in turn promotes metastases. On the other hand, Raf and c-Kit are a serin/threonin and a tyrosine-kinases, respectively, are involved in cell cycle progression and proliferation, both processes contributing to the tumor progression (see above for a description of the main molecular pathways changed upon HCC progression). Thus, Srf inhibits tumor cell proliferation and tumor angiogenesis and increases the apoptosis rate in several tumor models.

Srf is presently the most efficient treatment tested for HCC. However, the patient's quality of life is still severely impaired, both through side effects common to all chemotherapeutical medicaments (fatigue, weight loss, alopecia, myalgia…), that up to 79% Srf-treated HCC patients experiment, and specific to antiangiogenic agents[8]. Two typical adverse effects of Srf are palmar-plantar erythrodysesthesia, commonly known as "hand-foot skin reaction", and an increased heart failure risk, both attributed to the VEGFR inhibition: in the dairy activity hands, feet and coronary vessels are constantly subject to brusque pressure changes and thus suffer damage. However, upon Srf treatment the capacity to repair this small but continuous damage is impaired. Palmar-plantar erythrodysesthesia is extremely painful, while increased heart failure risk forces treatment withdrawal in some cases. Additionally, sustained Srf supply leads to multi-drug resistance (MDR)[9], and thus increases tumor aggressiveness. Srf is also highly hydrophobic and thus very poorly-soluble in aqueous solvents, which reduces its absorption efficiency in the gastrointestinal tract and results in turn in poor pharmacokinetics. Taken together, its low bioavailability and side effects have limited the clinical application of this antineoplastic compound in HCC. Although we center our study in the treatment of HCC, these drawbacks are common to many chemotherapeutical agents in different types of cancer.

This limitations have led researchers to pursue new alternative therapies. The ever expanding field of nanotechnology has tried to provide these alternatives through the encapsulation of antitumoral agents in biodegradable polymeric matrixes that allow controlling the release kinetics. Therefore, a controlled release of the medicament would allow

us to modify its administration procedures, achieving an increase of its concentration within the neoplastic tissue and reducing side effects in healthy organs.

Srf biodistribution improvement has followed different strategies. Regarding the encapsulation polymeric matrix used to achieve a sustained drug release, several biodegradable materials have been already tested, such as PLGA or lipids. Mieszawska and colleagues successfully encapsulated Srf in lipid and PLGA-composed nanoparticles in 2013 [10], forming an outstanding nanoparticle with Srf in its lipidic corona and Doxorubicin in the PLGA. Also, they could follow nanoparticle distribution in vivo thanks to the coencapsulation of gold nanoparticles within the PLGA matrix. Gao *et al.* followed a similar strategy two years later[11], and although they did not coencapsulate any other therapeutical drug nor any metal within the PLGA matrix, they achieved a successful target towards HCC tumors in vivo. PEG, used as nanoparticle coating, prevents nanoparticle removal from blood vessels by the mononuclear phagocytic system. This possibility has been explored by Cao [12], Dudek [13] and Liu [14]. Cao *et al* synthesized a nanoparticle formed by a vitamin E derivative coupled to PEG and enhanced it with Srf and curcumin for combinatorial therapy. Dudek *et al* approached the combination of free Srf with a nanoparticle coated in PEG whose target was β-catenin and demonstrated its efficacy *in vivo*. On the other hand, Liu synthesized a PEG-coated nanoparticle able to successfully transfect anti-HIF1α siRNA into tumor cells. Along with the polymer PLGA, poly-caprolactone nanoparticles have also been used to carry Srf. The use of lipidic nanoparticles carrying Srf has also been extensively investigated: Zhang *et al* created in 2014 [15] a "lipid coated nanodiamond" bearing a Srf cargo, using DSPE-PEG to coat the nanodiamond surface.

Srf can be combined with a plethora of medicaments and targeting molecules in order to increase either its concentration in the target tissue or its antiproliferative and antiangiogenic effect within cells. These are some of the strategies that have already been explored:

- Coencapsulation: Srf can be coencapsulated with other chemotherapeutical drugs, for example doxorubicin [10], [16] or paclitaxel [17]. Doxorubicin is also used as side-treatment when performing RFA ablation or TACE (see above).
  The coencapsulation of Srf and genetic material aiming for cancer gene therapy is especially related to the topic of the present work. Shen and colleagues [18] successfully coencapsulated Srf and anti-survivin shRNA in PEI-based nanoparticles and demonstrated its synergistic effects in HCC culture cells and in an *in vivo* HCC model. Moreover, they demonstrated their effect in preventing MDR, a widespread phenomenon upon Srf administration.

- Tumor targeting: Srf concentration can not only be increased in the tumor area, but also healthy organs may be avoided, through the targeting of disease upregulated molecules. Already studied targets include CRCX4[11] , the folic acid receptor [19], [20],[21] (FR), VEGFR and PDGFR [22] and the transferrin receptor [16], [23].

- Subcellular compartment targeting: it consists in increasing the drug concentration in the target subcellular compartment, through several strategies: i) Wang *et al* [24] were able to couple two derivatives of RGD to a Srf bearing nanoparticle. RGD binds to integrins and afterwards promotes release in the cytoplasm through its cleavage . ii) pH and/or redox status-responsive polymers: whenever nanoparticles enter the vesicle trafficking system within the cell, they are subjected to pH and redox status changes. Poly-HIS is responsive to pH [24] while polymers with disulfide bonds are

responsive to redox status changes (Gaspar et al 2015)[25]. pH- or redox-responsive particle disaggregation promotes cargo release within the cytosol. A whole plethora of polyethyleneimine (PEI) polymers has been issued in this sense. The endosomal escape mechanism can be consulted below.

Coming back to polymeric matrixes, PLGA is a polymer composed by lactic and glycolic acid monomers. Its swelling behavior and hydrolysis susceptibility are influenced by the molar ratio of its individual monomers. PLGA containing 50:50 ratio of glycolic and lactic acids undergoes hydrolysis much faster than those containing a higher proportion of either monomer. The glass transition temperature of PLGA copolymer is highly above physiologic temperature, and hence PLGA is considered to be sufficiently stable under these conditions[26].

PLGA is also highly biodegradable: the polymer chains undergo bulk degradation, which occurs at uniform rate throughout the polymer matrix, (facilitating drug escape through nanoparticle erosion, together with drug diffusion). Once the PLGA has been degraded to its monomeric units through cleavage of its backbone ester linkages (hydrolytic degradation, which occurs spontaneously in an aqueous environment), these are processed in regular metabolic pathways. Fermentation and the Krebs cycle are mainly responsible for the degradation of the lactic acid to water and CO_2. Glycolic acid is either excreted unchanged in the kidneys or enters equally the tricarboxylic acids pathway [26]. Environment pH acidification by PLGA degradation within the cell is of little significance, and it must be remembered that tumor environment is already acidic[27].

On the other hand, siRNA capacity to silence specific genes has generated great interest directed towards their use as therapeutic agents against a wide range of pathologies including cancer, infectious and metabolic diseases. Plasmid DNA carries exogenous DNA, which leads to mRNA transcription and ultimately to protein expression when introduced into cell nuclei. It is also a promising strategy for the treatment of multiple diseases.

However, there are several obstacles that must be overcome when attempting gene therapy. Due to their size and negative charge, nucleic acids do not readily pass through the also negatively-charged cell membrane. Another main limitation is DNA/RNA susceptibility to degradation by intra- and extra-cellular nucleases, which renders a short siRNA or DNA half-life. Given that siRNA are much shorter and stiffer than plasmid DNA, they are usually harder to complex into nanoparticles. To prevent unwanted non-specific interactions between nanoparticles and biomolecules, some nanoparticles include hydrophilic polymers such as polyethylene glycol (PEG) which also promotes evasion from the mononuclear phagocytic system and nanoparticle recirculation within the blood vessels [28].

Thus, release systems must be designed to protect the genetic material from a premature degradation in the blood, and also they should be able to efficiently transfer therapeutic siRNAs to target cells. A wide variety of viral- and non-viral-based systems have been developed in order to achieve an efficient and secure siRNA release. Viral-based systems are highly efficient but are neither safe nor technological- transfer easy, due to their oncogenic potential and immunogenic and inflammatory effects. Even though non-viral vectors are becoming increasingly important, most clinical assays have been carried out with viral vectors. It is common to direct siRNA against those factors enhancing tumor progression.

As it occurs in the case of non-viral vectors, as they rely on endosomal internalization, nanoparticles should also promote endosomal escape in order to avoid cargo degradation in the lysosomes. This can be achieved either by actively disrupting the endosomal membrane or provoking endosome swelling (see below for a complete explanation of the latter). For siRNA delivery, the nanocarrier must release its content in the cell cytosol; in contrast, plasmid DNA should be delivered to the nucleus in order to achieve successful transfection. Therefore, DNA bearing nanocarriers may need to remain intact longer. Nuclear penetration is another obstacle that hinders transfection efficiency. Regarding cancer cells, plasmid transfection is generally easier than in non-proliferative healthy cells, given that when cell division occurs the nuclear membrane is necessarily disrupted and re-formed in later stages. Through this process some genetic material present in the cytosol may be enclosed in the newly-formed nucleus[28].

The main non-viral vectors that have been employed in gene therapy are outlined below:

Lipid-based nanoparticles are the most commonly used non-viral transfection method. Several transfection reagents, including Lipofectamine ®2000, are lipid-based. These lipids permit the conjugation of targeting ligands on its surface. It has been demonstrated that the addition of cholesterol in those lipids promotes cell uptake. Lipid hydrocarbon tail properties have been demonstrated to play a role in cell membrane fusogenicity and are therefore to be optimized when formulating novel nanocarriers [28].

Inorganic nanoparticles have also been explored for gene therapy. Calcium phosphate nanoparticles enable gene delivery via co-precipitation into nanocrystals, and their main advantage is that they can be coupled to other polymers, such as PEG. Gold nanoparticles have also drawn much attention as they can not only be used for nucleic acids delivery but also with diagnostic purposes (the simultaneous capacity for therapy and diagnose is normally termed as “theranostics”). Moreover, gold nanoparticles’ surface can be modified by cationic groups. Some other materials, like SPIONS, have also been used with theranostic purposes. Quantum dots such as CdSe/ZnS nanoparticles can be used as fluorophores as well as gene therapy vehicle. Mesoporous silicas are materials crossed with multiple porous arranged in a honeycomb-like manner. In this case, the surface available for the genetic material is drastically increased[28]. Inorganic nanoparticles are disadvantageous in the sense that they are not biodegradable. However, they commonly achieve a high transfection efficiency.

The third kind of material commonly used for intracellular gene delivery is polymeric materials. Advantages of PLGA have been previously explained, although it can be directly used to carry genetic material through a simple or double emulsion process, more commonly employed polymers are often cationic and thus interact with nucleic acids to form polyplexes. Cyclodextrins are a class of water soluble molecules composed by 6-9 glucose residues arranged in a cone shape, which form a hydrophobic interior that can be modified to allow the nucleic acid to fit in. Dendrimers consist in a central core molecule attached to a high number of polymer “tentacles”. The stepwise method of their synthesis permits control over the branching process, offering additional attachment sites for targeting molecules or drug codelivery. Poly-lysine (PLL) was often employed coupled with PEG to prevent aggregation in

serum. However, PLL is unstable and fails to escape the endosome in some cases. PEI has been the obvious replacement for PLL [28].

The polyethyleneimine (PEI) is generally used in transfection studies, due its high primary, secondary and tertiary amine content. These provide a high positive charge to which negatively charged nucleic acids can electrostatically bind, which makes protocols for generating nucleic acids-based complexes extremely simple. Also, PEI solutions are extremely stable over time and again, due to the presence of many amino groups, chemical modifications are relatively easy. Moreover, PEI has been shown to play an important role during nanoparticle endosomal escape towards the cytoplasm. The so-called "proton-sponge effect", or endosomal swelling, was proposed by Behr in 1997[29]. According to this model, when the PEI enters via endosome (the cell trafficking vesicle system), it progressively suffers protonation as the carrying endosome develops into a lysosome. Due to its many nitrogen atoms, PEI buffering capacity promotes an increased influx of Cl^- ions into the vesicle, which in turn disturbs the osmotic equilibrium in such a way that more water must enter the endosome. A combination of the osmotic swelling and the PEI swelling causes the rupture of the membrane and the release of its contents in the cytoplasm (see Figure 1). It has also been proposed that PEI prevents DNA degradation from cytosolic nucleases. Although some researchers have stated their doubts on the accuracy and importance of the proton-sponge effect model, PEI is still considered one of the best vectors to deliver genes. PEI has even been subject to clinical trials in bladder cancer, pancreatic adenocarcinoma, and recurrent ovarian cancer[30].

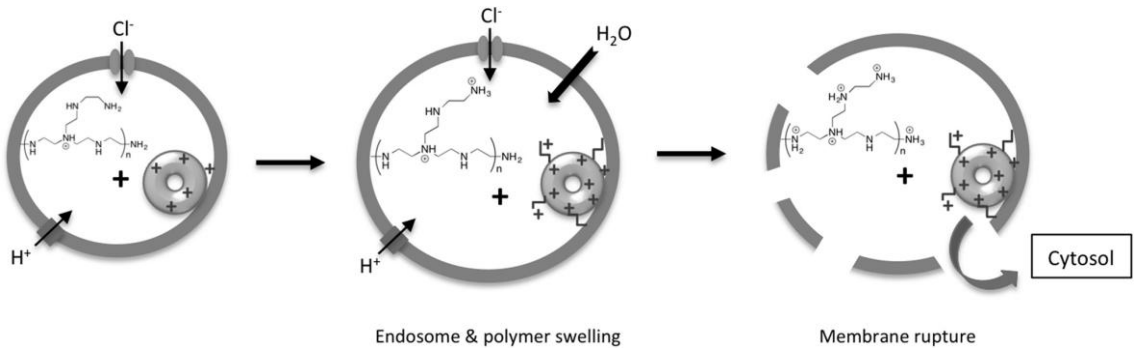

Figure 1: Proton-sponge effect as reviewed by Neuberg and Kirchler [31].

The objective of this master's thesis is to develop a nanoparticulated PLGA-based polymeric matrix that allows the simultaneous encapsulation of Srf and the attachment of either a plasmid or–siRNA molecules to its surface. In addition, once the nanoparticle endocytosis occurs, its release in the cytoplasm through the proton-sponge effect would be favored.

MATERIALS AND METHODS

Materials

The following chemicals were purchased from Sigma Aldrich: dymethyl sulfoxide (DMSO), phosphate buffered saline (PBS), Poly(D,L-lactide-*co*-glycolide) Resomer 503, Pluronic F68, acetone, *N*-(3-Dimethylaminopropyl)-*N*'-ethylcarbodiimide (EDC), *N*-Hydroxysuccinimide (NHS), 4-Morpholineethanesulfonic acid (MES), poly(ethyleneimine) 25KDa (PEI), 25KDa MWCO dialysis columns, potassium chloride (KCl), Phosphotungstic acid hydrate, acetonitrile and methanol. The following products were provided by Biowest: Eagle's Minimum Essential Medium (EMEM w/ stable glutamine, non-essential aminoacids, NEAA), glutamine, penicillin, streptomycin, amphotericin and Dulbecco's Phosphate Buffered Saline (DPBS). Fetal bovine serum was purchased from Thermo Fisher Scientific, and Sorafenib (Srf) was provided by Santa Cruz Biotech. The chemical structures of Srf, PLGA and PEI are shown in Figure 1.

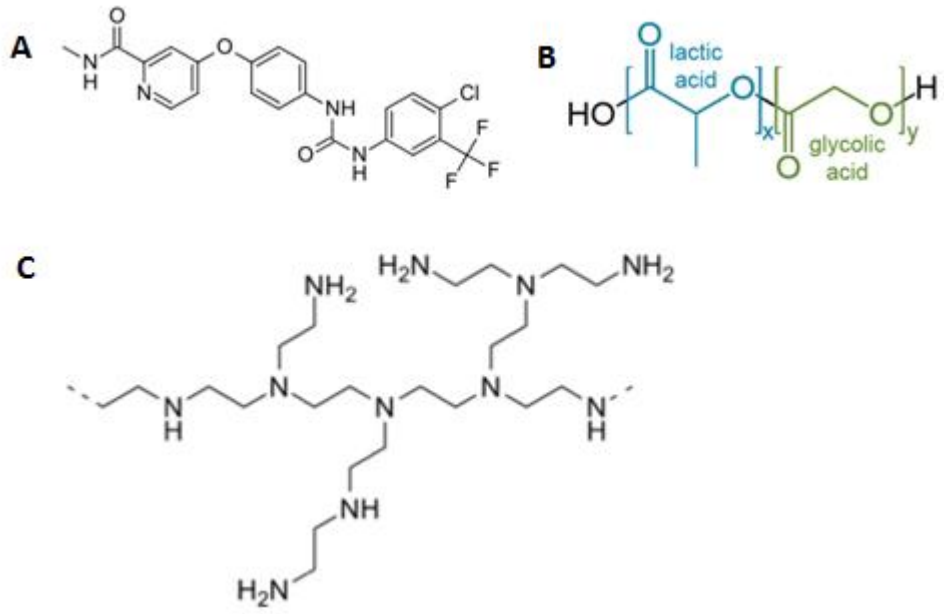

Figure 2: Chemical structures of A) Sorafenib B)PLGA and C) Branched PEI

Free Srf stability in organic/inorganic solvents at different temperature points

Srf stability in organic and inorganic solvents was assessed as following: two mixtures of Srf in either DMSO or DMSO: PBS 1X (1:2 v/v) were prepared and separately aliquoted. The Srf concentration, which was 16 µg/ml in DMSO and 14µg/ml in DMSO:PBS, was chosen as being the maximum detectable by UV-VIS spectrometry at 265 nm. Aliquots were kept either at room temperature or at 4ºC and measurements were performed on different time points through UV-VIS spectrometry.

Srf encapsulation in PLGA NPs

The polymeric material selected to encapsulate Srf was poly-lactic-glycolic acid (PLGA), a copolymer approved by the FDA in many devices and systems to administrate drugs thanks to its biocompatibility and biodegradability. We have selected the acid-terminated 50:50 (lactic acid: glycolic acid) variety, due to its low degradation relying on the ester bond hydrolysis and to its superficial negative charge and easy functionalization [26].

PLGA NPs were synthesized by simple emulsion-solvent evaporation method (o/w or oil-in water) in a continuous way, through the use of a microfluidic device designed with a "T"-shape (see Figure 3). A mixture of the desired drug and a polymeric matrix is dissolved in an organic solvent. The addition of a surfactant and the application of various forces (shear force, sonication, etc.) leads to the formation of an emulsion composed by organic nanodrops containing both drug and polymer and a surrounding immiscible inorganic phase. Evaporation is then promoted. As the vapor pressure of the organic phase is higher than that of the inorganic phase, the nanodrops' organic solvent is evaporated and the matrix and the drug come closer together precipitating thanks to the immiscibility of the organic solvent in water, finally forming nanoparticles dispersed in an aqueous phase.

Our microfluidic device comprises two confronted channels through which the inorganic phase flows, perpendicular to a third channel in which the organic phase flows. These channels are connected to three plastic Beckton Dickinson syringes placed on two Harvard Apparatus PHD Ultra pumps. Shear force stablished by the two confronted channels upon the perpendicular one is the driving force forthe formation of the nanodrops.

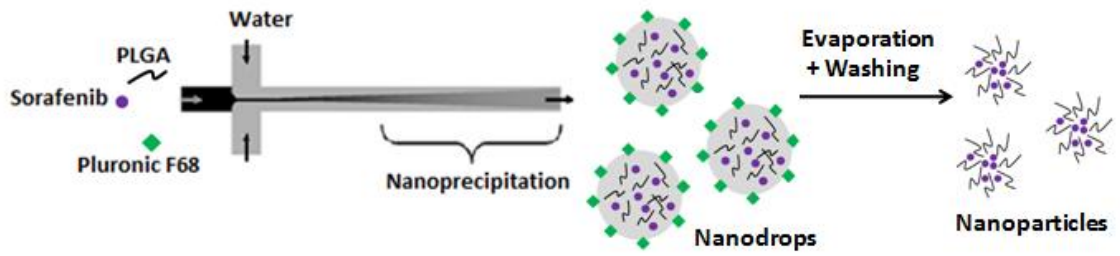

Figure 3: Srf PLGA cNPs synthesis scheme, modified from Valencia et al, 2008 [32].

The inorganic phase consists in MilliQ water and flows with a 10 ml/h flow rate. The organic phase consists in a 0,5% (w/v) PLGA Resomer 503, 2,5% (w/v) Pluronic F-68 and 5 or 10 % (wt/wt) Srf in acetone, with a 20 ml/h flow rate. The negative control was synthesized without Srf addition. The total volume of the synthesis is variable, but a 1:1 (v/v) correlation between the organic and inorganic phases must be maintained. Organic solvent evaporation is achieved through magnetic stirring at 600 rpm for 2 to 3 hours, a process called "nanoprecipitation". From now on we will refer to the resulting nanoparticlesas (Srf) PLGA NPs.

Srf PLGA NPs washing

Washing was performed by one-step centrifugation in Eppendorf tubes (1 ml of sample per tube) at 6.000 rpm for 30 min. Supernatant was removed and the pellet resuspended in 1 ml of either MilliQ water or 1x PBS, depending on the subsequent experiment.

Nanoparticle characterization

DLS and ZP measurements

Hydrodynamic diameter of the nanoparticles, particle size distribution and the polydispersity index were determined by Dynamic Light Scattering or DLS. Nanoparticles were resuspended 1:15 to 1:20 (v/v) ratio in distilled water and subsequently analyzed in a Brookhaven 90 Plus (Holtsville, NY) equipment. In order to determine the Zeta Potential, the samples were resuspended in a 1mM KCL dilution in a 1:60 to 1:100 (v/v) ratios and analyzed in the same equipment.

TEM images

TEM is employed to determine nanoparticle size, morphology and composition. Samples were deposited onto regular carbon-copper TEM grids and negative contrast was provided through a 3% (w/v) phosphotungstic acid hydrate dilution in distilled water. The equipment employed was a FEI TECNAI T20 TEM microscope, and the operational voltage was 200 kV.

Loading efficiency and drug loading

In order to determine the encapsulated Srf quantity within the PLGA nanoparticles, 1 ml sample was centrifuged at 11.000 rpm for 15 min. Once the supernatant had been removed, 1,15 ml 99,9% acetonitrile was added to the pellet and the vial was subjected to regular shaking for 30 min. 0,25 ml 99,9% methanol was added onto the acetonitrile and the vial was then sonicated for 15 min. Finally, a second centrifugation was performed at 12.000 rpm for 20 min and the supernatant transferred to a clean tube. Supernatant absorbance was then measured at 265 nm.

Loading efficiency and drug loading were defined as:

$$Loading\ efficiency\ (\%) = \frac{Drug\ mass\ within\ NPs}{Drug\ mass\ used\ in\ the\ synthesis} \times 100$$

$$Drug\ loading\ (\%) = \frac{Drug\ mass\ within\ NPs}{Total\ NPs\ mass} \times\ 100$$

Lyophilization

Nanoparticle lyophilization is necessary to prepare the samples for XPS Depth profiling, DSC and DSC analysis. Around 5 ml sample were submerged in liquid nitrogen until complete freezing. It was then subjected to high negative pressure overnight in a Telstar Lyoquest -55ºC lyophilizer.

XPS Depth profiling

XPS Depth profiling provides an atomic composition profile depending on the depth of the sample, which informs us where is the Srf placed within the PLGA nanomatrix. Sample preparation for XPS depth profiling analysis was prepared as follows: several sample drops were allowed to dry on a copper strip until achieving a thin film. The equipment used was an Axis Ultra from Kratos. Al monochromatic source was employed with working conditions 15 mA and 15 kV and pass energy 160 eV for the continuous spectrum and 20 eV in the different regions. A source for Ar ions clusters.was used for the etching.

DSC

In order to check nanoparticle behavior throughout a heating process, and thus obtain information on their composition, DSC measurements were performed with either a lyophilized sample (as previously described) or with powdered material used as controls in a DSC822^{e} Mettler Toledo equipment using 100 µl crucibles (no material in the reference crucible and around 3 mg in the sample crucible). An isothermal period of 2 min at 25ºC was followed by heating up until 600ºC with a heating rate of 10ºC/min.

FTIR

FTIR analysis provides information on the chemical bonds present in a sample. For FTIR analysis samples were lyophilized as previously described, whereas controls were carried out with dry powders. We used a Vertex 70 Brooker equipment with a Golden Gate ATR accessory. Measurements were performed between 4.000 and 600 cm^{-1} and the resolution obtained was 4 cm^{-1}.

Nanoparticle stability

Srf PLGA NPs were synthesized and washed as previously described and resuspended in 1X PBS (pH7,4). Samples were aliquoted and kept either at RT or 37ºC. DLS measurements and TEM analysis were performed on weeks 0, 1 , 2 and 5 to evaluate their morphology and potential fragmentation.

PEI coupling

In order to covalently attach polyethylenimine to the surface of the PLGA nanoparticles an EDC/NHS chemistry was performed to form a carbodiimide bond between the carboxylic group of the PLGA with the amino group of the PEI as following: 5 mg of previously synthesized PLGA NPs were mixed with 5 mg of EDC buffered in 10mM MES at pH 4,75 approximately. The mixture was incubated for 20 min at RT. Then 5 mg of NHS equally buffered in 10mM MES at pH around 4,5 was added to the previous mixture, and incubated for 10 min at room temperature. In order to remove the excess of EDC and NHS, the sample was then washed by one-step centrifugation for 20 min at 6.000 rpm. The pellet was then resuspended in MilliQ water and 1,25 mg of PEI 25 kDa buffered in PBS 1x at pH 7,75 approximately were added to the nanoparticle suspension and incubated at RT overnight.. Sample dialysis was then performed in 25kDa MWCO columns with 2,5 distilled water, which was refreshed each 12-18 h for 2 days, in order to remove the excess of PEI. Figure 4A depicts a scheme of the resulting nanoparticles Figure 4B displays a scheme of the EDC/NHS chemistry[33], EDC reacts with carboxylic acids groups to form an active O-acylisorurea intermediate that is easily displace by nucleophilic attack from primary amino groups present in the PEI, resulting in the formation of an amide bond between the carboxylic acid and the primary amine. A soluble urea derivative is released. However, the O-acylisourea is unstable. ECD couples NHS to carboxyls, forming an NHS ester that is more stable than the O-acylisourea.

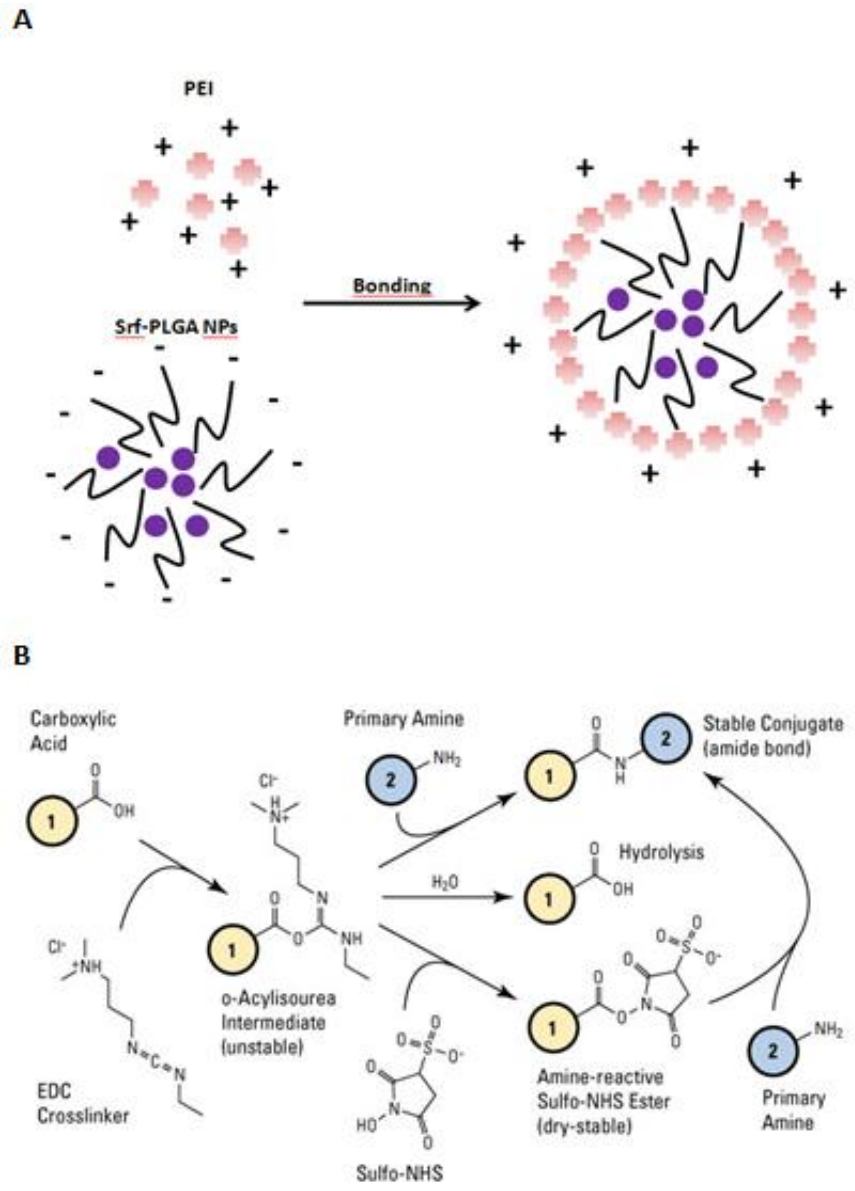

Figure 4: A). Srf PLGA cNPs bonding with PEI. B). EDC/NHS chemistry scheme, provided by ThermoFisher [33].

Figure 4A depicts an scheme of the resulting nanoparticles while Figure 2B shows the EDC/NHS chemistry

Cell culture

We chose HepG2 cell line for our assays, a line stablished on 1979 by Barbara Knowles *et al.* from a HCC obtained from a 15-year-old male. This cell line has been thoroughly characterized and is regularly used in metabolism, oncogenesis and hepatotoxicity studies. HepG2 cells were maintained in Eagle's Minimum Essential Medium (EMEM w/ stable Glutamine) supplemented with 10% (v/v) fetal bovine serum (FBS; Thermo Fisher Scientific), 1% (v/v) non-essential amino acids (NEAA), 2mM stable glutamine and the following antibiotics/antimycotics: 60 µg/ml penicillin, 100 µg/ml streptomycin and 0.25 µg/ml amphotericin B). HepG2 cells were washed with DPBS and incubated with fresh (2-4 days)

culture medium in a humidified 5% CO_2 atmosphere at 37ºC. Microraphies were taken with a Nikon Elipse TS100 optical microscope coupled to a Nikon D.Fi1 camera.

Cytotoxicity assays

Intrinsic nanoparticle cytotoxicity was determined through an Alamar Blue assay following the instructions provided by the manufacturer. HepG2 cells were seeded in MW96 plates with a 11.000 cells/well density (the number of cells per well was optimized prior to cytotoxicity assays) and were incubated in a humidified 5% CO_2 atmosphere at 37ºC for 24 h. Cells were then treated with either nanoparticles in a concentrations ranging from 0,01 to 0,5 mg/ml or with corresponding free Srf in regular complete culture medium. Cells were subsequently incubated for 16-24 h under the same conditions. Once the treatment had concluded, cells were washed with DPBS and incubated with 10% (v/v) Alamar Blue reagent in complete medium for 2-4 h. After this incubation period, emitted fluorescence was determined in a Biotek Synergy plate reader with an excitation wavelength of 530 nm and an emission wavelength of 590 nm. Cell viability is expressed as a percentage relative to the value obtained for the control cells.

RESULTS

Free Srf stability in organic/inorganic solvents at different temperature points

Srf is a drug administered via oral capsules of 200 mg each, being the total amount 800 mg of Srf tosylate per day. Still, as Srf is highly hydrophobic, we suspected that it may not be entirely stable in inorganic solvents. In order to determine Srf stability in inorganic and organic solvents, several aliquots of Srf dissolved in either DMSO or a mixture of DMSO and PBS were kept at room temperature or at a typical cold storage temperature of 4ºC. Srf concentration was determined at several time points. Results are depicted in Figure 5:

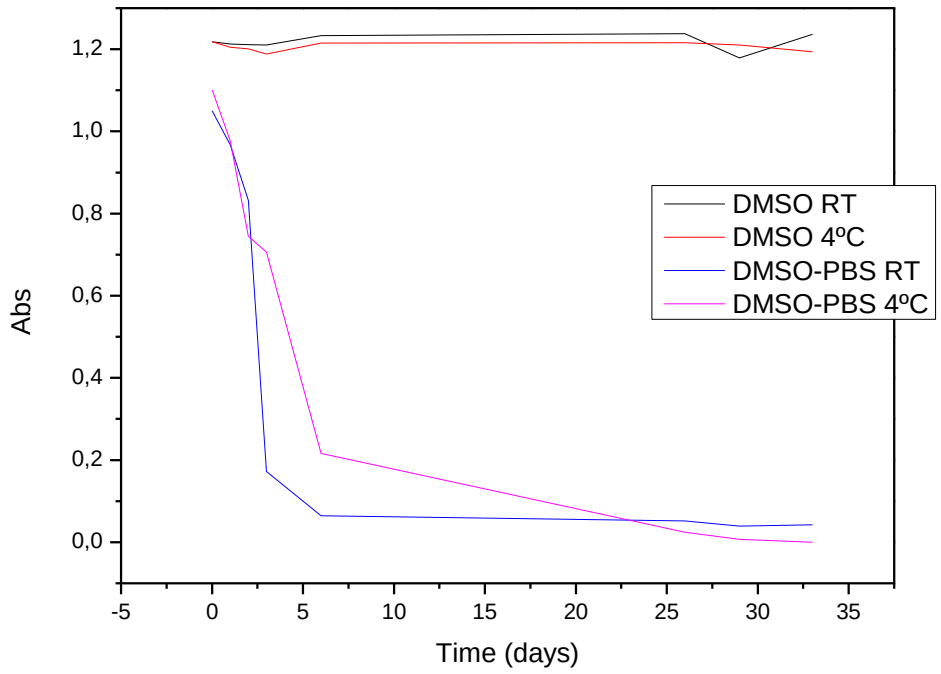

Figure 5: Srf stability in DMSO or DMSO:PBS at either 4ºC or RT

As shown in Figure 5, the absorbance of Srf dissolved in DMSO and kept at either room temperature or at 4ºC does not vary throughout the studied time. However, the absorbance of Srf dissolved in a mixture of DMSO and PBS and kept at either temperature rapidly decreases over time. The maximum is reached at time 0, and by day 5 more than 80% of the signal is lost. Moreover, by day 1 we can already observe a significant loss of 10% in the absorbance approximately. The loss seems to occur more rapidly at room temperature than at 4ºC. However, maintenance of the absorbance does not prove that the Srf is indeed active

From these results we can draw the following conclusions:

- Srf absorbance is little or not at all affected by the temperature it is being kept at when dissolved in DMSO.
- Srf absorbance is greatly influenced by the solvent in which it is dissolved. While in DMSO Srf concentration does not vary over time, it greatly does when in contact with an inorganic solvent such as PBS.

Our conclusions are that Srf is highly unstable in an inorganic solvent, and thus encapsulation within a polymeric matrix might prevent its degradation through time and thus may improve its storage and increase its bioavailability in the human plasma.

Nanoparticle synthesis and characterization

PLGA NPs synthesis optimization

Continuous nanoparticle synthesis was optimized by using different PLGA, Pluronic F-68 and Srf (w/w) ratios and concentrations. The results for the optimization of the PLGA and Pluronic ratios are summarized in Table 1. Formulations are presented in mg of PLGA and mg of Pluronic F68 per 2 ml of acetone (there is a variance both in ratios and in concentrations).

Table 1: PLGA NPs synthesis optimization

PLGA-Pluronic F68 (mg) in 2 ml organic phase	Mean diameter (nm)	Polydispersity Index	% population 1 / % population 2	Zeta Potential (mV)
10-30	75,61	0,146	95/5	-8,05±0,90
10-50	52,52	0,159	98/2	-30.67-±0,63
10-70	67,71	0,170	97/3	-30,65±1,80
10-90	51,21	0,029	97/3	-32,85±1,25
5-15	77,97	0,143	98/2	-8,45±0,14
5-30	68,30	0,157	98/2	-15,42±1,14
1-3	46,77	0,142	99/1	-9,44±0,36
1-30	59,24	0,147	98/2	- 9,16 ± 1,77

As it can be seen in Table 1, the formulations for which the mean diameter were lower were 10-50, 10-90 and 1-3.However, great differences could be observed in the Zeta potential values: while for the 10-50 and 10-90 the Zeta potential value was around -30 mV, for the 1-3 formulation it barely reached -10 mV.

The polydispersity index before washing by centrifugation is around 0,14 to 0,160 in most cases. The only value that differs is the one for the 10-90 mg formulation. Interestingly, in all of these syntheses (and the subsequent ones too) two nanoparticle populations could be found in the DLS distribution: the main one at about 50-60 nm and a second one between 200-400 nm, which will be termed as “Population 1” and “Population 2” from now on, respectively. Still, Population 2’s contribution to the total spectrum is negligible (Figure 7A) Even though the diameter of Population 2 is much higher that than of the Population 1, the number of NPs is so low that their contribution to the mean diameter of the total sample is negligible. Indeed,

Population 1 comprises about 98% of the sample in all cases. Anyhow, as the differences between the 1-50 and 1-90 formulations are minimal, we chose the 1-50 formulation because of its lower Pluronic F-68 surfactant content. Even though nanoparticles are washed before bonding with PEI, we are not able to remove all the Pluronic F-68, as shown in Figure 10B. The remnants of the surfactant may be disadvantageous when attaching PEI, surfactant may be placed on the nanoparticle surface and thus may hinder the carbodiimide reaction. That is mainly why we chose to use a lower quantity of Pluronic in the nanoparticle synthesis.

Interestingly, the washing step by centrifugation rendered an even a lower Zeta potential, achieving between 5 and 10 mV difference more (data not shown). We hypothesize that the excess of surfactant may be placed on the nanoparticle surface and thus reduces its negative charge.

Srf loading into PLGA NPs

The following step was to load Srf into the already optimized PLGA NPs. Prior to this step, we tested Srf solubility in acetone, as this solvent was not listed among those in which Srf is perfectly soluble [34]. Optimization of the Srf loading into the PLGA-based nanoparticles is resumed in Table 2.

Table 2: results the optimization of the Srf loading into the PLGA NPs.

Srf: PLGA (wt/wt) ratio	Diameter (nm) meas. by TEM	Polydispersity Index	%P1/ %P2	Zeta Potential (mV)	Drug loading (%)	Encapsulation efficiency (%)
1:10	50	0,099		-28,54 ± 1,84	8,8	46
1:20	45	0,101		-34,09 ± 1,06	6,7	78

According to the diameters measured by TEM imaging, they did not significantly differ from those obtained in unloaded PLGA NPs, with a diameter of approximately 40-50 nm, which also did not significantly vary between 1:10 and 1:20 formulations. Up to date we have not found any entry in the body of scientific literature that shows a Srf-loaded PLGA-based nanoparticle with such a reduced mean diameter, whether continuously or discontinuously synthesized. We believe that a lower diameter will help particle internalization[35] .

The polydispersity index was about 0,1 in both cases, what it is considered to be monodisperse[36]. Shockingly, this value is better than the one obtained for the unloaded nanoparticles, although it must be taken into account that in this case the polydispersity index is measured after nanoparticle washing. The monodispersity of the mixture was further confirmed by TEM imaging and by the distribution profile also obtained by DLS analysis (see Figure 6A and 6B). The lack of polydispersity also confirms that Srf PLGA NPs do not tend to aggregate in dispersion, what may have happened if any leftovers of Srf appeared on the nanoparticle surface (see Figure 6C). Monodispersity is also expected to be beneficial upon

drug release: when the sample has a wide range of nanoparticle diameters, nanoparticle erosion and drug release tend to be irregular and non-reproducible.

As the PLGA employed was acid-terminated, we were expecting to achieve nanoparticles with negative Zeta potential Indeed, the Zeta potential reached values between -25 and -35 mV. This negative Zeta Potential confirms the availability of carboxylic groups in the NPs for PEI bonding, and helps prevent NPs aggregation thanks to charge-based nanoparticle repulsion.

Values for drug loading were 8,8 wt.% for the 1:10 formulation and 6,7 wt.% for the 1:20 formulation. A great difference was obtained regarding the encapsulation efficiency, this is, the mass of drug actually enclosed within the resulting NPs as compared with the one used in the synthesis. While only less than 50% of the Srf used was encapsulated in the 1:10 formulation, more than 75% was encapsulated in the 1:20 formulation. Although a better result was obtained in the 1:10 formulation for the drug loading, in later replications we found this value to be highly variable. That, along with the outstanding encapsulation efficiency value and the non-significant differences in the mean diameters, polydispersity index and Zeta potential, is the reason why we chose the 1:20 formulation for the following experiments.

Srf PLGA NPs physicochemical characterization

A thorough characterization of the synthesized Srf PLGA NPs was performed next. TEM images confirmed sample monodispersity and mean diameter obtained by DLS. A thin film can be observed around the nanoparticle sample in some of the micrographies (Figure 6A). This is attributed to the sample contrast-providing treatment (see the Materials and Methods section) rather than to the sample itself. More importantly, all nanoparticles displayed a spherical morphology, which can be helpful in drug release (together with monodispersity as already stated). A spherical shape may help obtaining a more regular erosion of the nanoparticle and thus a better reproducibility in the drug release. It must be reminded that Srf is highly hydrophobic and that, when in contact with a polar solvent, absorbance (and consequently stability) rapidly decreases over time (see Free Srf stability in organic/inorganic solvents at different time points in the Results section). Thus, achieving a regular and constant release is of upmost importance.

DLS nanoparticle distribution (Figure 6B, Figure 7B) displays two nanoparticle populations in the range of 40-50 nm of diameter and 200 nm respectively, further confirming monodispersity and expected diameter. In this case, microscopy imaging and Dynamic Light Scattering analysis are coincident.

XPS Depth Profiling analysis was performed after lyophilization of the sample. XPS profile displayed an extremely high content in carbon (C) and oxygen (O), as expected of an organic polymeric sample. As they do not aport any extra information, the XPS Depth Profiling lines corresponding to C and O have not been included in Figure 6C. Each Srf molecule has 3 fluorine (F), 2 chlorine (Cl) and 4 nitrogen (N) atoms. As shown in Figure 6C, the three of them

can be found in all the scanned time points, this is, throught the whole length of the sample. Cl gives a very low signal, although its presence can still be confirmed within the Srf PLGA NPs. Although the values for the N seems to be increased over time of analysis, this can be attributed to the etching process rather than to a variance in the sample. It is with F that we can best analize the sample in terms of its spatial chemical composition. In this case, a roughly constant line between 0,2 and 0,4% of atomic concentration can be sketched through the whole analysis time. From this it can be concluded that the N, and thus the Srf, can be found throughout the whole sample at a constant concentration.

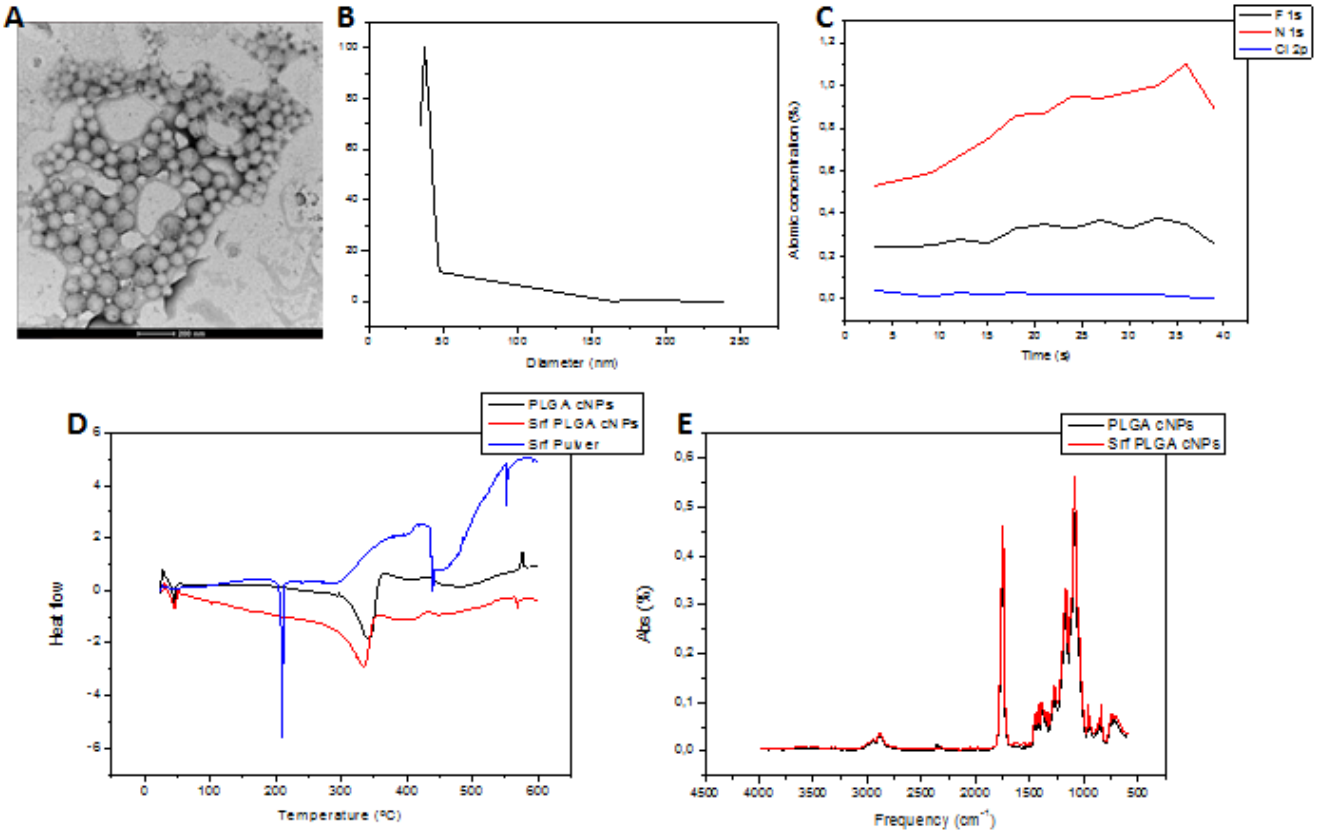

Figure 6: Srf PLGA NPs characterization. A) TEM micrograph. B) DLS diameter distribution. C) XPS Depth Field analysis. D) DSC profile. E) FTIR spectra

Differential Scanning Calorimetry or DSC analysis sheded interesting results. All meassurements started before PLGA glass transition temperature (40-44ºC). The first small peak both in the control PLGA NPs and in the Srf PLGA NPs can be attributed to this feature: although it is common to find such peaks in other materials at those temperatures in DSC, this peak is not present in the powdered Srf line. Regarding the line drawn from the Srf powder, the negative peak at arround 200ºC corresponds to the melting point of Srf (202 to 204ºC). The predicted boiling point for Srf is 523 ºC at 760 mmHg, according to the specification sheet provided by Santa Cruz Biotech (see Materials in Materials and Methods). A small negative peak appearing at around 550ºC may correspond to this event. Apart from that, results are less encouraging than expected. The profiles obtained for the PLGA and Srf PLGA NPs are highly similar. This means that the Srf contribution to the Srf PLGA NPs line is negligible. Given the high sensitivity of this technique, we may infere that only a very small quantity of Srf is enclosed within the PLGA matrix.

Figure 6E displays the FTIR spectra for unloaded PLGA NPs and loaded Srf PLGA NPs. As expected in a FTIR spectrum of organic materials, there is a high number of peaks between frequencies 1600 and 600 cm^{-1} that correspond to the stretching and bending vibrations of C-C and C-O bonds. A large peak at about 1700 cm^{-1}corresponds to the stretching vibrations of the C=O bond, in which PLGA, as a polymer comprised of acids, is rich. Another small peak between 3000 and 2500 cm^{-1} may correspond to the stretching vibrations of the C-H bonds. Strikingly, there is virtually no difference between the the spectra of the loaded and unloaded NPs. Drug loading and encapsulation efficiency were tested before sample lyophilization, and their values were similar to those displayed in Table 2. Even though we can therefore assure that Srf was present in the nanoparticles' sample, its contribution is not enough to form any supplementary peaks that explain the N-H bonds the Srf molecule has. This further confirms the results obtained by DSC. On the other hand, as no new peak is detected we can suppose that Srf is enclosed within the PLGA fibers of the nanoparticle and that the synthesis process does not provoke the formation of any additional bond. However this last statement must be carefully taken. As we are not even able to detect Srf, it is doubtful that bonds between Srf and PLGA could be detected with this sensitivity. Still, the synthesis process should rend unattatched Srf molecules.

In conclusion, we have obtained very small and monodisperse PLGA nanoparticles with a diameter about 50 nm bearing a Srf cargo of about 6-7 wt., in which no Srf can be found on the surface of the nanoparticle, but rather a conglomerate is formed between the Srf and PLGA with no apparent newly-formed bonding between them.

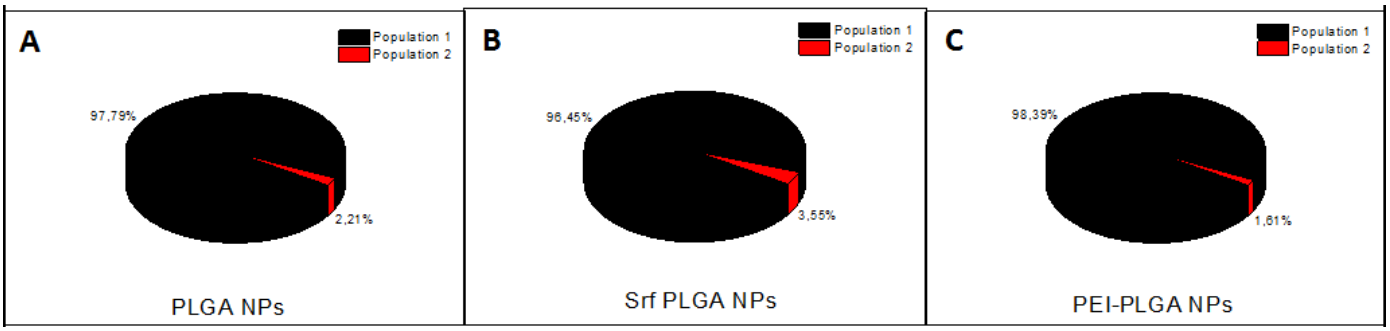

Figure 7: Percentages of Population 1 and Population 2 in A) unloaded PLGA NPs, B) loaded Srf PLGA NPs and C) PEI-coated (unloaded) PEI-PLGA NPs

Srf PLGA NPs stability

In order to test the stability of our nanoparticles in a tissue-resembling environment, Srf PLGA NPs were aliquoted and kept at either RT (control) or 37ºC. in PBS 1x. Several analysis were performed, including Zeta potential and DLS mean diameter measurements over time. While Zeta potential was maintained constant at all-time points both at RT and 37ºC (Figure 8A), mean diameter did change over time in a temperature-dependent manner (see Figure 8B). At RT a clear increase in the mean diameter can be traced. This can attributed either to

nanoparticle swelling or to nanoparticle aggregation due to the presence of salts contained in the Phosphate Saline Buffer which neutralize the electrokinetic potential which stabilizes the nanoparticles. Interestingly, the opposite trend was found when keeping Srf PLGA NPs at 37ºC: a progressive reduction of the mean diameter can be found from week 0 until week 5, what may be preferentially attributed to nanoparticle erosion and disintegration.

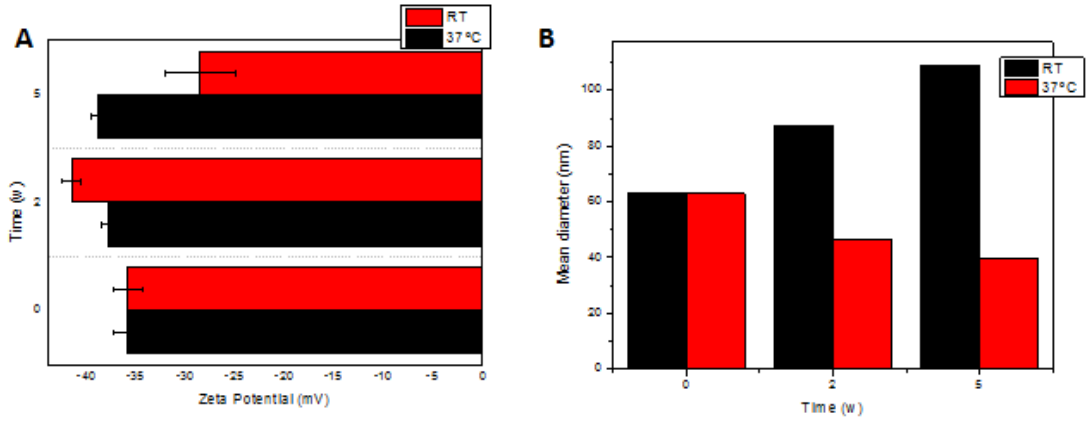

Figure 8: Stability of Srf PLGA NPs. A) Zeta potential and B) mean diameter variation over time

This hypothesis can be tested by simple distribution analysis. In order to differentiate nanoparticle swelling from nanoparticle aggregation, we can simply look at the variance of the nanoparticle populations. When aggregation occurs, it is feasible that the resulting agglomerates differ largely on their diameter, and still some unchanged separated nanoparticles should be found within the sample. However, if nanoparticle swelling occurs, two different populations with higher diameters than the ones measured at time point 0 should be present. This two populations were clearly discernible in the nanoparticle distribution obtained by DLS. Moreover, mean diameter clearly increases in a proportional way in both populations at RT and decreases at 37ºC, as displayed in Figure 9. We can thus conclude that temperature has a definite influence in Srf PLGA NPs swelling and erosion.

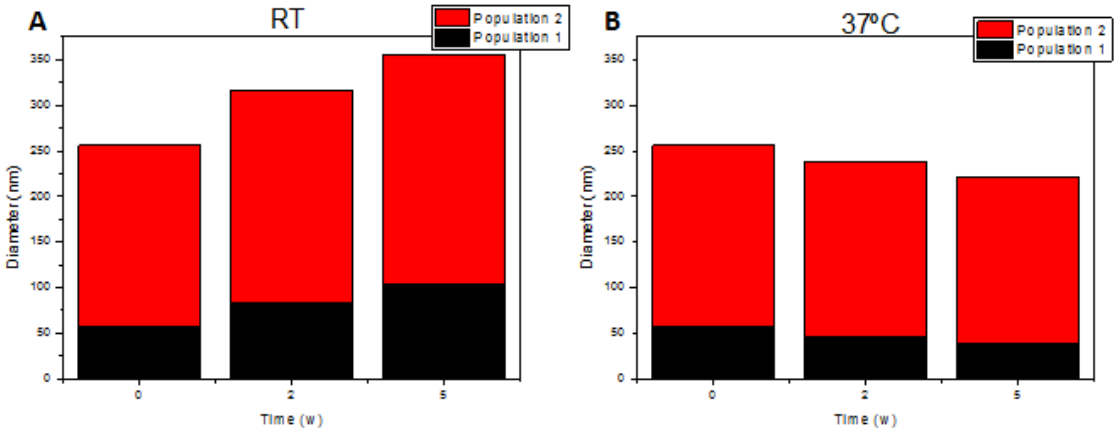

Figure 9: Nanoparticle diameter by population in stability assays in PBS suspended at A)RT and B) 37ºC.

PEI bonding to PLGA NPs

Next PLGA NPs were employed to achieve PEI covalent bonding to the nanoparticle surface through a ECD/NHS chemistry. An scheme of the reaccions involved in this process can be seen in Figure 4B, and the whole protocol can be consulted in "PEI coupling " in the Materials and Methods section. The coating of PLGA NPs with PEI was successfully achieved. As shown in Figure 10A, we were able to obtain a full reversion of the Zeta potential, having around -30 mV when the acidic PLGA is explosed on the surface of the nanoparticle (thanks to the carboxilic groups), to around +30 mV when PEI is attatched, thanks to its many protonated amine groups. This reversion is very encouraging, given that a high positive charge must be obtained in order to electrostatically bind the negatively-charged nucleic acids. The ribose/deoxyribose–phophate backbone provides this negative charge[37].

Moreover, FTIR analysis confirmed that a covalent bond was formed between the carboxilic groups of the PLGA and the amines of the PEI, giving rise to amide bonds (such as those occuring the in protein primary structure). Amide bonds should create a peak at about 1600 cm^{-1}. Indeed, such peak can be found in the PLGA NPs covered with PEI, but not in the untreated PLGA NPs nor in the PEI sample alone. FTIR spectra is depicted in Figure 10B.

As for the nanoparticle size, it seems that PEI attachment increases the nanoparticle mean diameter about a 40%. This is also confirmed by TEM imaging (Figure 10E). Interestingly, a second population with sizes ranging from 225 to 325 nm of diameter does appear in the DLS distribution (Figure 10D), what may lead us to think that PEI bonding provokes some nanoparticle aggregation. In contrast, the main population, comprised by nanoparticles with a rough diameter of 75nm, represents up to 98% of the total nanoparticles in the sample, and only 2% nanoparticles have a diameter comprised between 225 and 325 nm. As this is exactly what we had in the first place (see Figure 7), therefore, we can affirm no aggregation has occurred during the EDC/NHS chemistry, and monodispersity has been preserved throughout the process.

Moreover, TEM images (Figure 10E) show that PEI-PLGA NPs are also spherical, what may help attatch pDNA/siRNA regularly to the nanoparticles' surface. Remarkably, no difference in electronic density can be appreciated between the outter zone and the core of the nanoparticle, meaning that PLGA and PEI are too similar chemically to provoke any difference.

The following conclusions can be thus drawn from this set of experiments:

- PEI is covalently bound to the surface of the PLGA NPs
- PEI bounding provokes an increase in mean diameter and a reversion in the Zeta potential
- PEI bounding does not promote particle aggregation
- Nanoparticles preserve their spherical shape

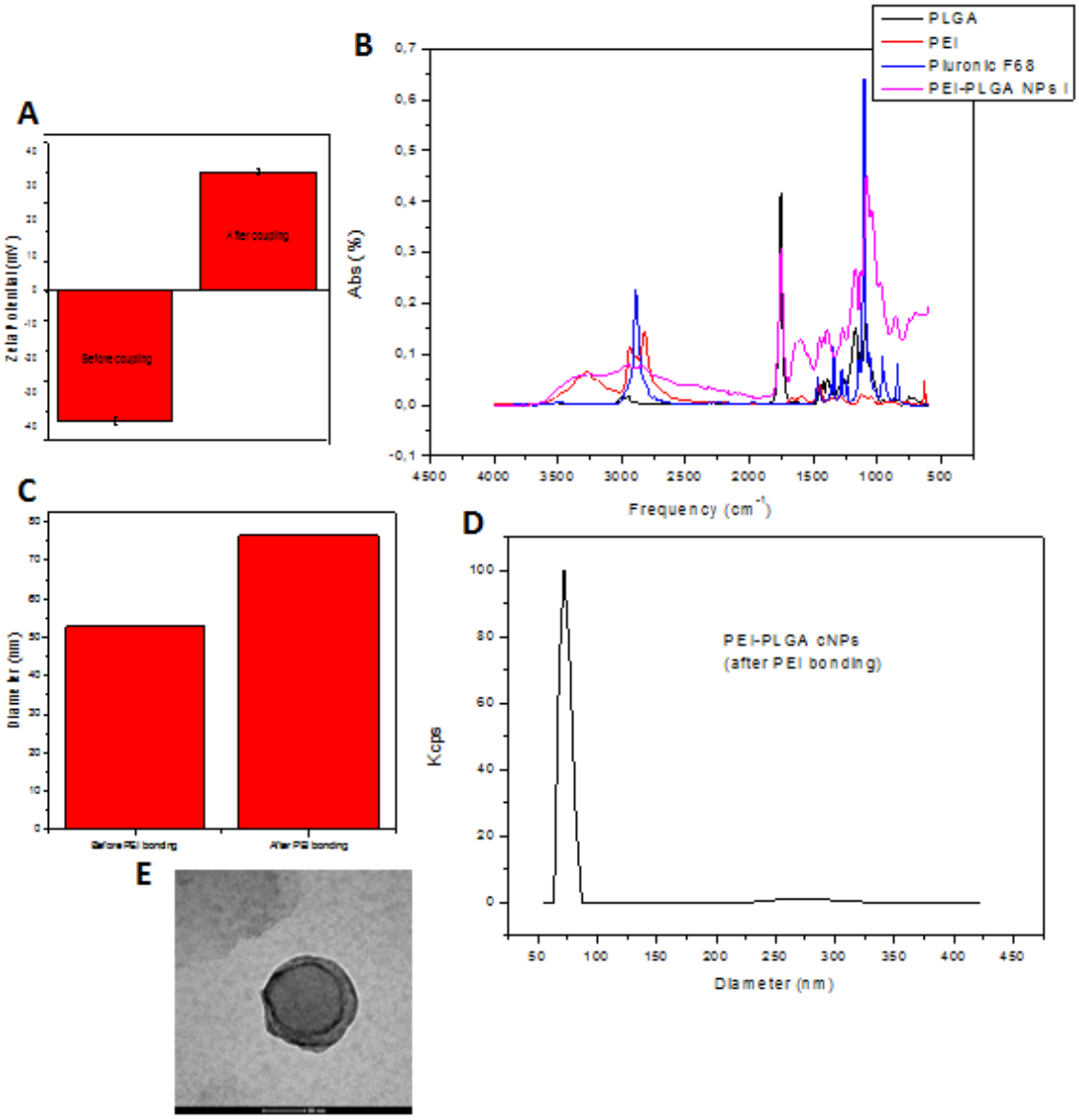

Figure 10: PEI bounding to PLGA NPs. A) Zeta potential variation. B) FTIR spectra C) Mean diameter variation D) DLS distribution E) TEM micrograph

Cytotoxicity tests in HepG2 cells

Srf PLGA NPs cytotoxicity was tested in HepG2 cells. Briefly, cells were seeded in 96 MW plates, treated for 24 h with different free Srf and Srf PLGA NPs and finally tested with Alamar Blue reagent (for a more detailed description of the Alamar Blue assay followed, please consult the subsection ” cytotoxicity tests in HepG2” in Materials and Methods.

Several considerations must be made before analyzing the cytotoxicity results. Cell density when seeding was optimized to achieve a regular and homogeneous monolayer of HepG2 cells in 96 MW plates prior to any assay. It must be taken into account that this cell line tends to grow in clusters, and that, in order to achieve a homogeneous distribution of the

treatment among the seeded cells, all of them must be in contact the culture medium. A micrograph 4X of HepG2 cells is shown in Figure 11A. It was also checked that a 2% (v/v) DMSO content in the culture medium did not have any negative effect on cytotoxicity nor impaired cell growth. It is also imperative to clarify that the quantity of free Srf added to the culture medium corresponds to that encapsulated within the Srf PLGA NPs at a given concentration, what allows us to compare the effect of the chemotherapeutical agent dispersed in the medium and enclosed within a PLGA-based nanoparticulated matrix.

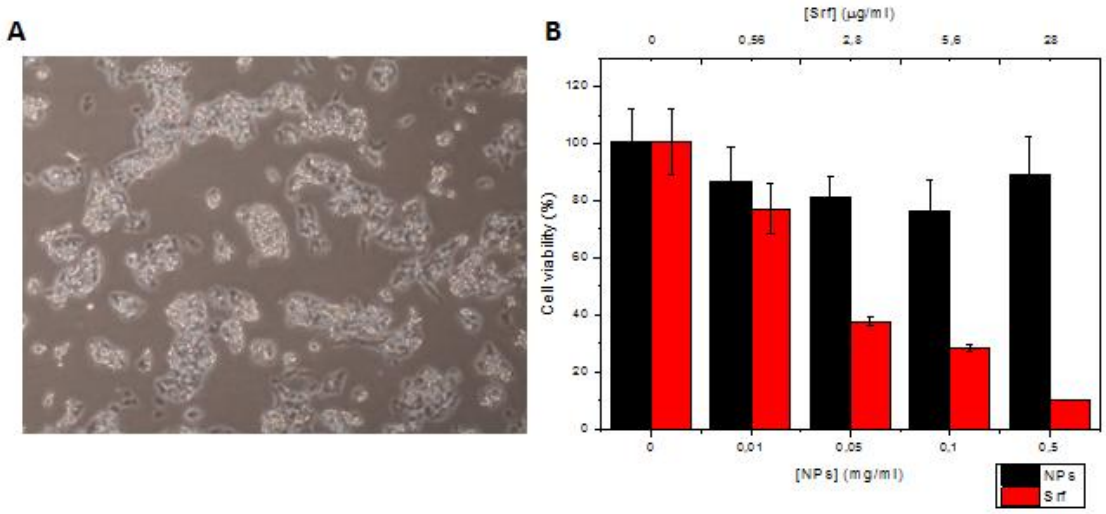

Figure 11: cytotoxicity test of Srf PLGA NPs in HepG2 cell. A) HepG2 cells micrograph, 4X. B) Free Srf (red) and Srf PLGA NPs (black) cytotoxicity results

As shown in Figure 11B, more than 80% of the treated cells survived the Srf PLGA NP treatment as compared with the control in all treatments. 80% is commonly considered to be the minimum cell viability acceptable to hold any treatment as non-cytotoxic. On the other hand, free Srf displayed a high toxicity: already with minimum doses, as we can clearly see with a 2,8 µg/ml concentration.

As all of the previous Srf PLGA NPs characterization relies either in desiccation or lyophilization of the sample, it can be argued that artifacts may be formed upon these processes and thus, it cannot be ascertained whether the Srf is indeed within the PLGA matrix or not. However, as proof of concept, this clearly demonstrates that Srf is in the interior of the NPs: if Srf was suspended in the solution (probably crystallized, given its high hydrophobicity), the Srf PLGA NPs sample would exert a similar effect as the free Srf treatment did. Moreover, even if Srf was partly encapsulated and partly free in the Srf PLGA NPs sample, some cytotoxicity might be obtained when testing high concentrations, which does not occur. In any case, we can affirm that Srf in indeed embedded in the PLGA matrix and that, if any remnants remain outside, they are not concentrated enough to exert any effect on HCC tumor cells.

Furthermore, we have demonstrated that the Srf PLGA NPs are not cytotoxic *per se*. Up to 0,5 mg/ml Srf PLGA NPs do not have any effect regarding cytotoxicity, and are therefore safe to use in our liver tumor model.

DISCUSSION

Free Srf stability in organic/inorganic solvents at different temperatures

Srf is a highly hydrophobic molecule[38]. This hydrophobicity is necessary for the molecule to block the ATP-binding pocket of its target kinase proteins: receptor tyrosine kinases are comprised by four main domains, namely the N-terminal extracellular ligand-specific binding site, a transmembrane domain, the intracellular ATP-binding region, to which an ATP molecule is recruited in order to perform phosphorylation, and a C-terminal intracellular activation loop which binds to the downstream signaling messengers. Srf is a type II inhibitor, meaning that it forms a hydrogen bond directly to the ATP-binding site even when the receptor is inactive and still in its monomeric form. This ATP binding cleft is highly hydrophobic. Specificity to the molecules listed in the Introduction is given by the part of the molecule not resembling the ATP [38] but this hydrophobicity is shared by several other kinase-targeting agents.

Anyhow, hydrophobicity is the main hallmark of Srf. According to our Srf provider, it is only soluble in DMSO, hot methanol, ethanol and ethyl acetate [34]. However, none of these solvents can be used alone when applying treatment to the culture cells. That is why we suspected that Srf could suffer changes in its chemical structure or undergo crystallization when diluted in an inorganic solvent.

Indeed, Srf concentration decreases over time when diluted in a mixture of PBS and DMSO. It must be noted that still in our experiments one third of the mixture is DMSO. Some DMSO is necessary in order to dissolve the Srf , but when administered in cell cultures DMSO volumes with respect to the culture medium are much lower, namely around 2% (v/v). That is why it is our guess that the loss may be even higher in regular culture medium.

Another factor that should be taken into account is that, in our system, no active removal of Srf occurs. However, Srf undergoes oxidative metabolism, mediated by CYP3A4, and UGT1A9-mediated glucuronidation in cells [38].

During systemic treatment several metabolites of Srf have been identified and it has been proven that Srf elimination half-time is between 25 and 48 h, and that it is secreted both in feces and in urine [38]. Although this time roughly corresponds with the loss observed in our experiment, it must also be noted that systemic-administration of Srf relies on its conjugation to form a salt, namely sorafenib tosylate, which is soluble in water (less than 1 mg/ml) at 25 °C.

Therefore, future experiments must assess if Srf tosylate concentration also decreases over time when diluted in an inorganic solvent, and if there is any significant difference between Srf and Srf tosylate effectiveness. In any case, Srf encapsulation within the PLGA

matrix may prevent its degradation and help providing similar results with lower quantities than the ones used with the free drug.

Nanoparticle synthesis and characterization

Nanoparticles of around 50 nm of diameter of a PLGA-based matrix were successfully synthesized. Nanoprecipitation consists on diluting a polymer or block-copolymer in an organic solvent, forming with the aid of a surfactant an oil-in-water (O/W) emulsion in which the polymer is located in the organic nanodroplets and letting the organic solvent evaporate. Polymer fibers are forced in this way to collapse, and finally the polymeric nanoparticle is formed. Nanodrop emulsion can be obtained in either a discontinuous, for example applying an ultrasound pulse to the organic/inorganic mixture, or a continuous way, with the aid of a microreactor. Surfactant addition in either phase usually helps to create the nanodrops.

As the quantities of the synthesized sample can be easily varied with no further optimization, we decided to use a continuous approach. The method presented by Valencia and colleagues on 2008 [32] was subtly changed in order to obtain our desired NPs. We first strived to change the original solvent, acetonitrile, for a less toxic one, namely acetone. Even though several washing steps took place after nanoparticle formation, such as centrifugation and dialysis, we did not want to jeopardize cytotoxicity on behalf of solvent traces. We checked that nanoparticle was even lower when using acetone instead of acetonitrile as solvent (mean diameter 31,14 nm as by DLS analysis). Also, in order to be able to covalently bond PEI to the nanoparticle surface, a high amount of carboxylic residues should be available. That is the main reason why PLGA-PEG block copolymer could not be employed as in the original article, but rather an acid-terminated PLGA should be used. PEG is an amphiphilic molecule, meaning that when PEG concentration is above the so called critical micelle concentration (cmc), micellar nanodroplets tend to appear, being the interaction of the soluble blocks and the solvent responsible for the stabilization of the micelles [39]. However, in the absence of PEG, it is the poloxamer Pluronic F68 the one that provides an amphiphilic platform thanks to which the PLGA and Srf-containing organic phase and the inorganic phase can be stabilized upon nanodroplet formation.

Up to date we have not found any other Srf-bearing PLGA-based nanoparticles as small in diameter as the ones presented in this work. Kim *et al.* [40] were able to synthesize a dextran-PLGA nanoparticle loaded with Srf, being its Zeta potential equal to that of ours (around -35mV) and the mean diameter 63 ± 0.58 nm, higher than those we have obtained when loading Srf, which are about 40-50 nm, as shown in Figure 6B. We hypothesize that a reduction in nanoparticle mean diameter should lead to a higher nanoparticle internalization rate. Drug loading is much lower (less than 2%, as compared with our 6,7%), as well as loading efficiency (around 25%). Unluckily, cytotoxic effects cannot be compared, given that neither the assay nor the cell type are coincident.

Even though diameter is augmented upon PEI binding (diameter around 70 nm, Figure 10D), we still have achieved to synthesize nanoparticles much smaller than most of those already reported, with the additional feature of being able of both delivering a chemotherapeutical agent and providing a platform for gene therapy. We hypothesize that this

low diameter should promote nanoparticle endocytosis and the PEI should help endosomal release, which are critical steps in cargo delivery to subcellular compartment. As stated before, Srf targets either cytosolic molecules or the cytosolic part of receptor proteins, and siRNA must be delivered to the cytosol in order to find their AGO complex and trigger specific mRNA degradation. Plasmidic DNA should enter the cell nucleus after leaving the endosome. Still, these hypotheses should still be challenged in further experiments.

Some comments must be made on our nanoparticles being able to perform gene therapy. As stated in Materials and Methods and throughout the Results part, we have not yet attached siRNA or pDNA to the PEI-PLGA NPs surface. However, we have already performed such experiments in PLGA- composed nanoparticles with PEI on their surface, with the difference that these nanoparticles had been synthesized in a discontinuous way by applying ultrasounds to the mixture and were therefore higher in diameter (data not shown). Both siRNA and pDNA were successfully bound to the nanoparticle surface, achieving a Zeta potential reduction of about 15mV (data not shown). Binding between the nucleic acids and the PEI-PLGA NPs was achieved through sheer electrostatic interactions. As this union is extremely simple, we are confident that we will be able to repeat and optimize this process with the continuously synthesized PLGA nanoparticles.

PEI has also been shown to be highly cytotoxic. We thus rely on our dialysis method to prevent any trace of unbound polymer from affecting HCC cells and on siRNA/pDNA successful coating to disguise the high positive charge of the nanoparticles.

Cytotoxicity tests in HepG2 cells

HepG2 cell line has been extensively characterized and is widely used in toxicology and cancer-related studies, especially for the former. HepG2 was used as our HCC *in vitro* model, to test whether our Srf PLGA NPs had an intrinsic cytotoxic effect on these cells, and to compare the cytotoxicity of Srf enclosed within the polymeric matrix or diluted in culture medium. As expected, Srf PLGA NPs did not display any cytotoxic effect to a concentration up to 0,5 mg/ml, while a quantity of free Srf corresponding to 0,05 mg/ml of NPs resulted in 60% of cell mortality. Unfortunately this cytotoxicity cannot be compared with other published tests, given that they are not coincident in either nanoparticle nature, cell line or cytotoxicity test method employed.

It must be noted that, even though apparently free Srf could reach cells more easily, in an *in vivo* model all cells would equally suffer the effects of this treatment, regardless of the cell type. However, Srf PLGA NPs should accumulate in the tumor vessels thanks to the so called EPR effect: as tumor vessels are aberrant, they usually leave fenestrations big enough for the nanoparticles to pass through, and thanks to which nanoparticles are passively targeted to the tumor.[41] We This is why we believe our nanoparticles will have enhanced delivery effects *in vivo*. Also, as Srf is highly hydrophobic [38] cell internalization may be impaired at the cell membrane level, while NPs should enter the cell via endocytosis, overcoming this obstacle.

.

CONCLUSIONS

The conclusions of this work can be summarized as follows:

1. Srf concentration decreases in inorganic solutions over time, but not in organic solutions. This decrease happens independently of the temperature.
2. Srf can be loaded onto PLGA nanoparticles of about 50 nm of diameter, with Srf comprising around 6-7% of the nanoparticle total weight. Nanoparticles formed are spherical in shape and have a negatively charged surface (-35 mV). The sample is monodisperse, being comprised by a main population (97-98%) of nanoparticles with 40-50 nm of diameter and a second population (2-3%) with 200-300 nm.
3. The Srf is embedded in the PLGA matrix forming no additional bonds and it is evenly distributed throughout the entire nanoparticle volume, though it is not localized on the nanoparticle surface.
4. Srf PLGA nanoparticles suffer either swelling or erosion over time in inorganic solutions depending on the temperature.
5. PEI can be covalently attached to the surface of the PLGA nanoparticle through an EDC/NHS chemistry that forms an amide bond between the carboxylic groups of the PLGA and the amine groups of the PEI. This procedure increases the nanoparticle diameter in about 20 nm (diameter reaches about 70 nm) and reversal of surface charge rends a positively charged nanoparticle (about +35 mV). The spherical shape of the nanoparticle is kept and the process promotes no nanoparticle aggregation. Two nanoparticle populations arise from this process, resembling the ones obtained in the PLGA NPs sample. The sample preserves its monodispersity.
6. Srf PLGA NPs have no intrinsic cytotoxicity in an HCC-derived (HepG2) monolayer cell culture, up to a concentration of 0,5 mg/ml after 24h of treatment.

FUTURE WORK

As already stated, future experiments must be carried out in order to improve, characterize and test *in vitro* our nanoparticles. Some of the experiments that must be necessarily undertaken are listed below:

1. siRNA and pDNA surface electrostatic binding: we expect to couple siRNA and pDNA to the nanoparticle surface taking advantage of their negative charge, which should electrostatically bind to the positively-charged PEI-PLGA NPs. For this we will optimize the quantity of nucleic acid added to the nanoparticle dispersion by electrophoresis and determine the Nitrogen/Phosphorus ratio by XRD.
2. Cytotoxicity test of siRNA and pDNA bound nanoparticles: in order to determine if the generated nanoparticles have intrinsic cytotoxic effects on HepG2 cells, we will test their cytotoxicity through Alamar Blue test at different concentrations..
3. Transfection optimization and evaluation of the silencing/transfection ability of our nanoparticulated vectors compared to commercially available reagents: several transfection experiments will be performed, with different concentrations and times. Transfection efficiency will be determined using a reporter Green Fluorescent Protein (GFP) –bearing plasmid by confocal microscopy, while silencing efficiency will be assessed by Western Blot and reverse PCR.
4. Synthesis of the Srf loaded siRNA/pDNA bound nanoparticle and test *in vitro:* once the drug loading and the transfection parameters have been optimized, nanoparticles loaded with Srf and coupled to siRNA or pDNA will be synthesized and characterized using the same techniques already described.

These experiments will all be performed within the author's starting PhD thesis with the support of a grant issued by the *Diputación General de Aragón* (DGA).

BIBLIOGRAPHY

1. Dhir M, Melin AA, Douaiher J, et al. A Review and Update of Treatment Options and Controversies in the Management of Hepatocellular Carcinoma. *J Korean Med Sci*. 2016;18(3):979-985. doi:10.3109/00365521.2016.1166518.

2. Poulou LS, Botsa E, Thanou I, Ziakas PD, Thanos L. Percutaneous microwave ablation vs radiofrequency ablation in the treatment of hepatocellular carcinoma. *World J Hepatol*. 2015;7(8):1054-1063. doi:10.4254/wjh.v7.i8.1054.

3. Adhoute X, Penaranda G, Raoul JL, et al. Usefulness of staging systems and prognostic scores for hepatocellular carcinoma treatments. *World J Hepatol*. 2016;8(17):703. doi:10.4254/wjh.v8.i17.703.

4. Turnes J, Díaz R, Hernandez-guerra M, et al. Decisiones terapéuticas en el tratamiento del carcinoma hepatocelular y patrones de uso de sorafenib. Resultados del estudio internacional observacional GIDEON en España. *Gastroenterol Hepatol*. 2015;38(4):263-273. doi:10.1016/j.gastrohep.2014.11.001.

5. Shin JW, Chung Y. Molecular targeted therapy for hepatocellular carcinoma : Current and future. 2013;19(37):6144-6155. doi:10.3748/wjg.v19.i37.6144.

6. Herbst DA, Reddy KR. Risk Factors for Hepatocellular Carcinoma. *Clin Liver Dis*. 2012;1(6):180-182. doi:10.1002/cld.111.

7. Wilhelm S, Carter C, Lynch M, et al. Discovery and development of sorafenib: a multikinase inhibitor for treating cancer. *Nat Rev*. 2007;5:17-19. doi:10.1038/nrd2130.

8. Doyle A, Marsh P, Gill R, et al. Sorafenib in the treatment of hepatocellular carcinoma: a multi-centre real-world study. *Scand J Gastroenterol*. 2016;51(8):979-985. doi:10.3109/00365521.2016.1166518.

9. Zhai B, Sun XY. Mechanisms of resistance to sorafenib and the corresponding strategies in hepatocellular carcinoma. *World J Hepatol*. 2013;5(7):345-352. doi:10.4254/wjh.v5.i7.345.

10. Mieszawska AJ, Kim Y, Gianella A, et al. Synthesis of Polymer − Lipid Nanoparticles for Image-Guided Delivery of Dual Modality Therapy. *Bioconjug Chem*. 2013.

11. Gao DY, Lin TT, Sung YC, et al. CXCR4-targeted lipid-coated PLGA nanoparticles deliver sorafenib and overcome acquired drug resistance in liver cancer. *Biomaterials*. 2015;67:194-203. doi:10.1016/j.biomaterials.2015.07.035.

12. Cao H, Wang Y, He X, et al. Codelivery of Sorafenib and Curcumin by Directed Self-Assembled Nanoparticles Enhances Therapeutic E ff ect on Hepatocellular Carcinoma. *Mol Pharm*. 2015. doi:10.1021/mp500755j.

13. Dudek H, Wong DH, Arvan R, et al. Knockdown of β -catenin with Dicer-Substrate siRNAs Reduces Liver Tumor Burden In vivo. *Mol Ther*. 2014;22(1):92-101. doi:10.1038/mt.2013.233.

14. Liu XQ, Xiong MH, Shu XT, Tang RZ, Wang J. Therapeutic delivery of siRNA silencing HIF-1 alpha with micellar nanoparticles inhibits hypoxic tumor growth. *Mol Pharm*. 2012;9(10):2863-2874. doi:10.1021/mp300193f.

15. Zhang Z, Niu B, Chen J, et al. The use of lipid-coated nanodiamond to improve bioavailability and efficacy of sorafenib in resisting metastasis of gastric cancer. *Biomaterials*. 2014;35(15):4565-4572. doi:10.1016/j.biomaterials.2014.02.024.

16. Malarvizhi GL, Retnakumari AP, Nair S, Koyakutty M. Transferrin targeted core-shell nanomedicine for combinatorial delivery of doxorubicin and sorafenib against hepatocellular carcinoma. *Nanomedicine Nanotechnology, Biol Med*. 2014;10(8):1649-1659. doi:10.1016/j.nano.2014.05.011.

17. Zhang J, He B, Qu W, et al. Preparation of the albumin nanoparticle system loaded with both paclitaxel and sorafenib and its evaluation in vitro and in vivo. *J Microencapsul*. 2011;2048(October 2015). doi:10.3109/02652048.2011.590614.

18. Shen J, Sun H, Meng Q, et al. Simultaneous Inhibition of Tumor Growth and Angiogenesis for Resistant Hepatocellular Carcinoma by Co-delivery of Sorafenib and Survivin Small Hairpin RNA. *Mol Pharm*. 2014.

19. Wang C, Sarparanta MP, Ermei MM, et al. Multifunctional porous silicon nanoparticles for cancer theranostics. *Biomaterials*. 2015;48:108-118. doi:10.1016/j.biomaterials.2015.01.008.

20. Li Y, Dong M, Kong F, Zhou J. Folate-decorated anticancer drug and magnetic nanoparticles encapsulated polymeric carrier for liver cancer therapeutics. *Int J Pharm*. 2015;489:83-90. doi:10.1016/j.ijpharm.2015.04.028.

21. Ling D, Xia H, Park W, et al. PH-sensitive nanoformulated triptolide as a targeted therapeutic strategy for hepatocellular carcinoma. *ACS Nano*. 2014;8(8):8027-8039. doi:10.1021/nn502074x.

22. Noh GT, Kim M, Suh J, et al. Sunitinib – CLIO Conjugate : A VEGFR / PDGFR-Targeting Active MR Probe. *Mol Imaging Biol*. 2014;(November 2013):340-349. doi:10.1007/s11307-013-0697-9.

23. Retnakumari AP, Hanumanthu PL, Malarvizhi GL, et al. Rationally Designed Aberrant Kinase-Targeted Endogenous Protein Nanomedicine against Oncogene Mutated / Ampli fi ed Refractory Chronic Myeloid Leukemia. *Mol Pharm*. 2012;(Cml).

24. Wang CF, Mäkilä EM, Kaasalainen MH, et al. Copper-free azide-alkyne cycloaddition of targeting peptides toporous silicon nanoparticles for intracellular drug uptake. *Biomaterials*. 2014;35(4):1257-1266. doi:10.1016/j.biomaterials.2013.10.065.

25. Gaspar VM, Baril P, Costa EC, et al. Bioreducible poly (2-ethyl-2-oxazoline) – PLA – PEI-SS triblock copolymer micelles for co-delivery of DNA minicircles and Doxorubicin. *J Control Release*. 2015;213:175-191. doi:10.1016/j.jconrel.2015.07.011.

26. Jain RA. The manufacturing techniques of various drug loaded biodegradable poly (lactide- co -glycolide) (PLGA) devices. *Biomaterials*. 2000;21.

27. Thoma CR, Zimmermann M, Agarkova I, Kelm JM, Krek W. 3D cell culture systems modeling tumor growth determinants in cancer target discovery. *Adv Drug Deliv Rev*. 2014;69-70:29-41. doi:10.1016/j.addr.2014.03.001.

28. Kozielski KL, Rui Y, Green JJ. Non-viral nucleic acid containing nanoparticles as cancer therapeutics. *Expert Opin Drug Deliv*. 2016;13(10):1475-1487. doi:10.1080/17425247.2016.1190707.Non-viral.

29. Behr J. The Proton Sponge: a Trick to Enter Cells the Viruses Did Not Exploit. *Chim 51*. 1997;2(1):34-36.

30. Benjaminsen R V, Mattebjerg MA, Henriksen JR, Moghimi SM, Andresen TL. The Possible " Proton Sponge " Effect of Polyethylenimine (PEI) Does Not Include Change in Lysosomal pH. *Mol Pharm*. 2013;21(1):149-157. doi:10.1038/mt.2012.185.

31. Neuberg P, Kichler A. *Recent Developments in Nucleic Acid Delivery with Polyethylenimines, Chapter 9*. Vol 88. Elsevier; 2014. doi:10.1016/B978-0-12-800148-6.00009-2.

32. Valencia P, Basto P, Gu F, et al. Novel synthesis of polymeric nanoparticles for drug delivery applications using microfluidic rapid mixing. 2008:1513-1515.

33. Scientific T. Carbodiimide Crosslinker Chemistry. www.thermofisher.com.

34. Sorafenib | CAS 284461 - 73 - 0 | Santa Cruz Biotech. https://www.scbt.com/scbt/product/sorafenib-284461-73-0. Published 2016.

35. Prabha S, Zhou W, Panyam J. Size-dependency of nanoparticle-mediated gene transfection : studies with fractionated nanoparticles. *Int J Pharm*. 2002;244:105-115.

36. Dynamic Light Scattering Common Terms Defined. *Malvern Instruments Ltd*. 2011:1-6.

37. Thomas TJ, Riahi HAT, Thomas T. Polyamine – DNA interactions and development of gene delivery vehicles. *Amino Acids*. 2016. doi:10.1007/s00726-016-2246-8.

38. Gotink KJ, Verheul HMW. Anti-angiogenic tyrosine kinase inhibitors : what is their mechanism of action ? *Angiogenesis*. 2010:1-14. doi:10.1007/s10456-009-9160-6.

39. Karayianni M, Pispas S. *Self-Assembly of Amphiphilic Block Copolymers in Selective Solvents*.; 2008. doi:10.1007/978-3-319-26788-3.

40. Kim DH, Kim M, Choi C, Chung C, Ha SH, Kim CH. Antitumor activity of sorafenib-incorporated nanoparticles of dextran/poly(dl-lactide-co- glycolide) block copolymer. *Nanoscale Res Lett*. 2012:1-6.

41. Blanco E, Shen H, Ferrari M. Principles of nanoparticle design for overcoming biological barriers to drug delivery. *Nat Biotechnol*. 2015;33(9):941-951. doi:10.1038/nbt.3330.